Version: 03.04.2020

Ultrasmall gold nanoparticles (2 nm) can penetrate and enter cell nuclei in an in vitro 3D brain spheroid model

Viktoriya Sokolova,[a] Goodwell Nzou,[b] Selina B. van der Meer,[a] Tatjana Ruks,[a] Marc Heggen,[c] Kateryna Loza,[a] Nina Hagemann,[d] Florian Murke,[e] Bernd Giebel,[e] Dirk M. Hermann,[d] Anthony J. Atala,[c] and Matthias Epple,[a*]

[a] Inorganic Chemistry and Center for Nanointegration Duisburg-Essen (CeNIDE), University of Duisburg-Essen, Essen, 45117, Germany

[b] Wake Forest Institute for Regenerative Medicine, Wake Forest School of Medicine, Winston-Salem, NC, 27101, USA

[c] Ernst Ruska-Center for Microscopy and Spectroscopy with Electrons, Forschungszentrum Jülich GmbH, 52425 Jülich, Germany

[d] Chair of Vascular Neurology and Dementia, Department of Neurology, University Hospital Essen, University of Duisburg-Essen, Hufelandstraße 55, 45122 Essen, Germany

[e] Institute for Transfusion Medicine, University Hospital Essen, University of Duisburg-Essen, Hufelandstr. 55, 45122 Essen, Germany

Abstract

The neurovascular unit (NVU) is a complex functional and anatomical structure composed of endothelial cells and their blood-brain barrier (BBB) forming tight junctions. It represents an efficient barrier for molecules and drugs. However, it also prevents a targeted transport for the treatment of cerebral diseases. The uptake of ultrasmall nanoparticles as potential drug delivery agents was studied in a three-dimensional co-culture cell model (3D spheroid) composed of primary human cells (astrocytes, pericytes, endothelial cells). Multicellular 3D spheroids show reproducible NVU features and functions. The spheroid core is composed mainly of astrocytes, covered with pericytes, while brain endothelial cells form the surface layer, establishing the NVU that regulates the transport of molecules. After 120 h cultivation, the cells self-assemble into a 350 µm spheroid as shown by confocal laser scanning microscopy. The passage of

different types of fluorescent ultrasmall gold nanoparticles (core diameter 2 nm) both into the spheroid and into three constituting cell types was studied by confocal laser scanning microscopy. Three kinds of covalently fluorophore-conjugated gold nanoparticles were used: One with fluorescein (FAM), one with Cy3, and one with the peptide CGGpTPAAK-5,6-FAM-NH_2. In 2D cell co-culture experiments, it was found that all three kinds of nanoparticles readily entered all three cell types. FAM- and Cy3-labelled nanoparticles were able to enter the cell nucleus as well. The three dissolved dyes alone were not taken up by any cell type. A similar situation evolved with 3D spheroids: The three kinds of nanoparticles entered the spheroid, but the dissolved dyes did not. The presence of a functional blood-brain barrier was demonstrated by adding histamine to the spheroids. In that case, the blood-brain barrier opened, and dissolved dyes like a FITC-labelled antibody and FITC alone entered the spheroid. In summary, our results qualify ultrasmall gold nanoparticles as suitable carriers for imaging or drug delivery into brain cells (sometimes including the nucleus), brain cell spheroids, and probably also into the brain.

Keywords

Gold; Nanoparticles; Spheroids; Cytotoxicity; Neurovascular Unit; Blood brain barrier

Introduction

Many diseases affected the human brain. For instance, brain tumors, aneurisms, stroke and pathological depositions of proteins are of major clinical relevance. The neurovascular barrier (blood-brain barrier; BBB) efficiently protects the brain from xenobiotics which would otherwise enter via the blood stream [1-5]. The neurovascular barrier is very selective. It is mainly composed of endothelial cells connected by tight junctions (TJs) and adherent junctions (AJs) that restrict the entry of foreign molecules [2, 6-8]. Furthermore, it contains active transport channels such as permeability glycoproteins that export substances that would be toxic to the brain parenchyma [9], and enzymes like monoaminooxidases, transpeptidases and transferases that metabolize possible BBB penetrant toxins [10].

It is challenging to quantitatively assess the penetration ability of therapeutics, hence animal experiments with complex subsequent evaluation procedures are usually performed. However, over 95% of therapeutics from animal models fail to show efficiency in clinical trials. Consequently, different *in vitro* cell culture models have been developed in the last years to simulate the blood-brain barrier outside an animal model [11-17]. In trans-well approaches, a

two-dimensional co-culture of relevant cells simulates the blood-brain barrier. Much less studied, but closer to reality, are three-dimensional spheroid models that consist of three or more cell types [8, 13, 15-18]. In this case, the blood-brain barrier is simulated by the outer layer of different spheroid which prevents the transmigration of drugs or particles from the cell culture medium ("the blood") into the core ("the brain") [8, 15, 17].

The therapeutic application of nanoparticles for drug delivery or imaging in the brain is strongly restricted by the blood-brain barrier. In the literature different kinds of nanoparticles have been synthesized and applied *in vivo*, but the results are not very consistent and range from an almost unrestricted crossover of large nanoparticles (>100 nm) to very low targeting efficiencies into the brain (<0.1%) [19-23]. Besides the therapeutic aspect, there is also a considerable interest in nanotoxicology concerning the unintended transport of nanoparticles into the brain where they could induce harmful effects [24-26].

There is a broad consensus that particle size, shape, charge, and surface functionalization are the decisive parameters for the interaction of nanoparticles with cells and tissues [27, 28]. Among nanoparticles, ultrasmall gold nanoparticles have gained particular interest due to their small size that ranges between molecules and common biomolecules like proteins [26, 29-41]. In contrast to "classical" noble metal nanoparticles with a diameter of 10 nm [29, 31, 32, 42-44] or polymeric nanoparticles with a size around 70 nm [18], ultrasmall gold particles (<2 nm) have a particular potential to cross the neurovascular barrier due to their small size [37, 45-47]. They are also readily taken up by cells, and in some cases are even found in the cell nucleus [41, 48].

To investigate this in detail, we prepared and characterized well-defined ultrasmall gold nanoparticles for application in 2D and 3D cell culture models. We coupled fluorescent dyes (by click chemistry) and peptides (via cysteine) to their surface. A most useful feature of such nanoparticles is that they do not cause fluorescence quenching in contrast to "classical" larger nanoparticles [37], i.e. confocal laser scanning microscopy is well applicable to follow their pathway.

Experimental

Chemicals

Tetrachloroauric acid ($HAuCl_4$) was prepared by dissolving elemental gold (≥99%) in *aqua regia*. Sodium borohydride ($NaBH_4$, ≥96%), (+)sodium L-ascorbate (≥99%), copper(II)sulfate pentahydrate (≥99%), and tris(3-hydroxypropyl-triazolyl-methyl)amine (THPTA, ≥95%) were

obtained from Merck (Darmstadt, Germany). Dipotassium hydrogen phosphate and potassium phosphate were obtained from Panreac Applichem. Amino guanidine hydrogen carbonate (≥98%) was obtained from Alfa Aesar. Fluorescein alkyne (≥95%, FAM-alkyne; 5-isomer) and sulfo-cyanine-3-alkyne (≥95%, Cy3-alkyne) were obtained from Lumiprobe. The tripeptide 6-azido-lysine-cysteine-asparagine K(N_3)CD (≥95%) was obtained from EMC Microcollections (Tübingen, Germany).

For the synthesis of peptide-functionalized gold nanoparticles, solid tetrachloroauric acid sodium salt ($NaAuCl_4$; Merck, ≥99%) was dissolved in water. The reduction was performed by sodium borohydride ($NaBH_4$, ≥96%) in the presence of the synthetic peptide CGGpTPAAK-5,6-FAM-NH_2 (≥95%), that was obtained from Caslo Aps (Kongens Lyngby, Denmark).

Ultrapure water with a specific resistivity of 18.2 MΩ (Purelab ultra instrument from ELGA) was used for all synthesis and purifications. Before use, all glassware was cleaned with boiling aqua regia and thoroughly washed with ultrapure water afterwards.

Instruments

We performed confocal laser scanning microscopy (CLSM) with a TCS SP8 AOBS system operated by the LASX software (Leica Microsystems, Wetzlar, Germany). The laser lines used for excitation were Diode 405 nm (DAPI; detection range 410-460 nm), Argon 488 nm (FAM, detection range 488-520 nm), DPSS 514 nm (Cy3; detection range 535-561 nm), and HeNe 633 nm (Alexa Fluor 647; detection range 640-720 nm). Images were acquired with HC PL Fluotar 10x/0.3, HC PL APO 20x/0.75 CS2, and HCX PL Apo 63x/1.4 oil objectives. Imaging conditions: pinhole 1 AU, laser intensity 5%. The spheroid images were all recorded with the same set of parameters.

The cell viability (live/dead assay, see below) was determined by fluorescence microscopy. A Keyence Biorevo BZ-9000 instrument (Osaka, Japan), equipped with filters for FITC and TRITC with 10x and 20x objectives were used. All images were recorded with the BZ-II viewer software and further processed with the BZ-II analyzer software.

Synthesis of dye-clicked nanoparticles (Au-Click-FAM and Au-Click-Cy3)

The synthesis and click reaction of the ultrasmall gold nanoparticles were performed as reported earlier [48]. Briefly, the ultrasmall gold nanoparticles were prepared by a modified one-phase Brust synthesis, followed by copper-catalyzed azide-alkyne cycloaddition (CuAAC).

For gold nanoparticles terminated with azide groups, the cysteine- and azide-containing peptide K(N_3)CD (4.5 µmol) was dissolved in 6 mL water and the pH was adjusted to 7 by adding 0.1 M sodium hydroxide solution while stirring continuously. The solution was degassed with argon and 30 µL 50 mM tetrachloroauric acid ($HAuCl_4$, 1.5 µmol) was added. After the yellow color of the $HAuCl_4$ had disappeared, 22.5 µL of a 200 mM ice-cold aqueous sodium borohydride solution ($NaBH_4$, 4.5 µmol) were injected to the flask. After adding $NaBH_4$, the solution quickly turned brown, and the dispersion was stirred at room temperature for another hour.

The CuAAC was performed with the unpurified azide-terminated gold nanoparticle dispersion as follows: 112.5 µL of 20 mM alkyne fluorophore solutions (either FAM-alkyne or Cy3-alkyne) were mixed with the dispersed azide-terminated nanoparticles. To avoid by-products of an undesired side reaction of reactive carbonyl compounds, 2.7 mL of a 20 mM solution of aminoguanidine in potassium phosphate buffer (0.05 M, pH 8) were added to the reaction mixture. Then, 600 µL of the solution were injected into a mixture of 200 µL of 20 mM copper(II) sulphate and 400 µL of 50 mM THPTA. Finally, the addition of 500 µL of 100 mM sodium ascorbate solution produced the catalyzing Cu(I) complex for the click reaction. The dispersion was stirred overnight at room temperature in inert atmosphere (argon). The dispersion was then passed through an ultrafiltration spin column (MWCO 3 kDa, 15 mL; Amicon®; Merck) for 20 min at 14,000 g to remove all unreacted compounds. After centrifugation, the filter was rinsed with potassium phosphate buffer (0.05 M, pH 8) until the filtrate was clear. The concentrated gold nanoparticles (~1 mL) were recovered from the filter with a pipette.

Synthesis of peptide-functionalized nanoparticles (Au-CGGpTPAAK-FAM)

The synthesis was done under full inert gas atmosphere (argon). For gold nanoparticles coated with the synthetic fluorophore-labelled peptide CGGpTPAAK-5,6-FAM-NH_2 (5,6-carboxyfluorescein; denoted short as CGGpTPAAK-FAM in the following), 1.5 µmol of peptide was dissolved in 2 mL degassed water and the pH was adjusted to 8. Then, 0.02 mL of $NaAuCl_4$ (0.5 µmol) was added to the peptide solution under stirring. After 10 min of cooling the mixture in an ice bath, 0.01 mL of $NaBH_4$ (2 µmol, freshly dissolved in 4 °C cold water) was added and stirred for another hour. Purification was done by spin filtering with an Amicon spin filter (MWCO 3 kDa, 0.5 and 2 mL; Amicon®; Merck) for 15 min at 14,000 g. The nanoparticles were washed with potassium phosphate buffer solution (0.05 M, pH 8) until the

filtrate was colorless (the dispersed gold nanoparticles had a slightly brown color). The resulting volume of concentrated nanoparticle dispersion was in the range of 0.05-0.06 mL. Recovery was accomplished by centrifugation at 1,000 g for 2 min [49].

Quantification of the amount of nanoparticle-conjugated molecules

The concentration of the clicked FAM-alkyne, Cy3-alkyne, and fluorophore-labelled peptide was determined by quantitative UV spectroscopy and fluorescence spectroscopy after a calibration with the free fluorophore-labelled ligands at the following wavelengths: FAM-alkyne (λ_{ex}= 485 nm), Cy3-alkyne (λ_{ex}= 550 nm), and CGGpTPAAK-FAM (λ_{ex}= 485 nm). Based on a particle diameter of 2 nm (solid core by HRTEM), the following numbers of attached molecules per nanoparticle were computed: 9 FAM-alkyne molecules and 5 Cy3-alkyne molecules by UV-vis spectroscopy, and 5 CGGpTPAAK-FAM molecules by fluorescence spectroscopy. UV-vis spectroscopy was carried out with a Varian Cary 300 instrument in Suprasil® quartz glass cuvettes with a sample volume of 600 µL. Fluorescence spectroscopy was carried out with an Agilent Technologies Cary Eclipse Spectrophotometer from 500 to 700 nm. A 96-well black flat bottom microplate with a sample volume of 300 µL was used. For control experiments, the same concentrations of dissolved dye molecules as delivered in gold-conjugated form were applied. Absorption and fluorescence spectra are given in the Supplementary Information (Figures S1, S2, S3).

Cells and cell culture conditions

Human primary brain microvascular endothelial cells (hpBECs; Creative Bioarray, New York USA) were expanded in plates pre-coated with gelatin-based coating solution (Creative Bioarray) for 2 min and cultured under normal growth condition (37 °C with 5% CO_2) in endothelial cell growth medium (ECM) with 5% FBS, endothelial growth supplements (ScienCell Research Laboratories, Carlsbad, USA) and penicillin-streptomycin. Human primary pericytes (hpPs; ScienCell Research Laboratories) were expanded in plates coated with 15 µg mL^{-1} poly-L-lysine (Merck) for 2 h and cultured under normal growth conditions in pericyte medium (PM; ScienCell Research Laboratories) supplemented with 2% FBS, pericyte growth supplements (ScienCell Research Laboratories) and penicillin-streptomycin. Human primary astrocytes (hpAs; ScienCell Research Laboratories) were expanded in plates coated with 15 µg mL^{-1} poly-L-lysine (Merck) for 2 h and cultured under normal growth conditions in astrocyte medium (AM; ScienCell Research Laboratories) supplemented with 2% FBS,

astrocyte growth supplements (ScienCell Research Laboratories) and penicillin-streptomycin. hpBECs, hpPs and hpAs were used in the experiments between passages 2 and 4.

Before application the cells were analyzed by flow cytometry to validate their mesenchymal or endothelial origin. The measurements were performed on a CytoFlex instrument (Beckman Coulter, Krefeld, Germany) and analyzed by FlowJo (BD Biosciences, Heidelberg, Germany). Briefly, the cells were stained for 30 min at 4 °C using panels of different antibodies (see Supplementary Information, Figure S4 and Table T1). Dead cells were excluded by 7-AAD staining (Beckman Coulter). All cells showed the expected mesenchymal/endothelial cell surface phenotypes.

3D spheroid culture

We followed the protocol reported earlier in refs. [8, 13, 15, 17] to prepare 3D spheroids. hpBECs, hpPs and hpAs were harvested using TrypLE select enzyme (1X, Thermo Fisher, Dreieich, Germany). To demonstrate the self-assembly of spheroids, the hpBECs were labelled by CellTracker™ Green CMFDA (Thermo Fisher), the hpPs were labelled by CellTracker™ Red CMTPX (Thermo Fisher) and the hpAs were labelled by CellTracker™ Deep Red (Thermo Fisher) according to the manufacturer's instructions. The cells were cultured in ultra-low attachment 96-well plates (ULAPs; Corning, Germany). The spheroids were allowed to form in spheroid medium, containing 3000 cells (1000 hpBECs, 1000 hpPs, and 1000 hpAs) per spheroid. 60 µL of the cell suspension supplemented with 0.3% rat tail collagen type I solution (BD Bioscience) was dispensed into each well of the 24 well ULAPs. Plates were then incubated under standard conditions for 72-120 h. Spheroids were harvested and fixed (4% paraformaldehyde; Merck) before CLSM.

Cell Viability

The cell viability was evaluated by a Live/Dead™ Cell Imaging Kit (Thermo Fisher) according to the manufacturer's protocol. Human brain spheroids were harvested for cell viability analysis after 120 h of incubation. Spheroids were incubated at room temperature for 10 min in Dulbecco's phosphate-buffered saline (DPBS) containing 2 µM calcein AM solution (green: living cells) and 4 µM ethidium homodimer-1 solution (red: dead cells). After washing once with DPBS, the spheroids were imaged with a Keyence Biorevo BZ-9000 instrument (Keyence, Osaka, Japan).

Immunostaining

The spheroids were collected in 2 mL Eppendorf tubes. After aspirating the media, the spheroids were fixed in 4% paraformaldehyde (Merck) for 15 min at 4 °C and washed 3 times with cold DPBS. The spheroids were exposed to 0.1% Tween-20 in PBS for 30 min followed by 3 washing steps with cold DPBS. Blocking was performed with 10% normal donkey serum in PBS/0.025% Tween-20 for 1 h at RT. The spheroids were incubated at 4 °C overnight in DPBS/0.025% Tween-20 containing the primary antibodies, i.e. anti-CD31 (1:100, Abcam), anti-ZO-1 (1:100, Invitrogen), PDGF-R-β (1:50, Cell Signaling Technologies), GFAP (1:100, Invitrogen), β-Catenin (1:100, Cell Signaling Technologies), P-gp (1:50, Invitrogen), and Desmin (1:100, abcam). The spheroids were subsequently washed 3 times and incubated with AF488 donkey anti-rabbit, AF555 donkey anti-mouse and AF647 donkey anti-rat (for triple staining) or AF488 donkey anti-rabbit and AF594 donkey anti-rat (for double staining) (1:600, Thermo Fisher) in blocking solution for 2 h at room temperature including Hoechst33342 solution (1:1000, Thermo Fisher) for nuclear staining. The spheroids were washed and transferred to 8-well chamber slides. Images were collected by CLSM using a Zeiss AxioObserver.Z1 combined with an LSM 710 confocal instrument. At least three randomly chosen spheroids were imaged for each stain.

Permeability assay

One group of spheroids was incubated in media under normal growth conditions with a FITC-conjugated anti-mouse F4/80 antibody (1:200, BioLegend, Germany) or 100 nM FITC solution (Merck) for 30 min. In a control group, the spheroids were treated with 4.5 mM histamine solution (Merck) 15 min prior to incubating with FITC-conjugated anti-mouse F4/80 antibody or 100 nM FITC for 30 min. The spheroids were washed three times before imaging by CLSM.

Nanoparticle uptake studies in a 2D co-culture cell model

For the uptake studies, hAs, hPs and hBECs were trypsinized and seeded in a Nunc™ Lab-Tek™ II 4-Chamber Slide™ System (Thermo Fisher) with a density of 9000 cells per well: 3000 hpBECs, 3000 hpPs and 3000 hpAs in 180 µL medium. Before seeding cells for the experiment, they were labelled with CellTracker dyes (Thermo Fisher) according to the manufacturer's instructions. After 120 h of incubation, the nanoparticle dispersions were added to the 2D co-cultures (Table 1). As control, the cells were incubated with the dissolved dye at the same concentration. After 24 h, the whole cell culture medium was removed with a pipette

and the cells were fixed with 4% paraformaldehyde solution at room temperature for 10 min, followed by washing for three times with DPBS. For labelling nuclei, the cells were then stained with DAPI and washed three times with DPBS. Finally, the cells were studied by CLSM. To identify the location of the nanoparticles within the cells, z-stacks were acquired (step size 0.2 µm).

Table 1: Parameters of gold nanoparticles applied to 2D and 3D cell culture models. The first value applies to 2D cell culture (9000 cells per well), and the second value applies to 3D cell culture (3000 cells per well). For control experiments with the dissolved dyes, the same dye concentrations as with the nanoparticles were used. Pep-FAM = CGGpTPAAK-FAM.

	Au-Click-FAM	**Au-Click-Cy3**	**Au-Pep-FAM**
	2D / 3D	2D / 3D	2D / 3D
c(Au stock dispersion) / µg µL^{-1}	0.50	0.50	0.25
V(medium) per well / µL	180 / 60	180 / 60	180 / 60
V(Au stock dispersion) per well / µL	9 / 3	9 / 3	18 / 6
m(Au) per well / µg	4.5 / 1.5	4.5 / 1.5	4.5 / 1.5
c(Au) in well / µg µL^{-1}	0.025	0.025	0.025
Particles (*d*=2 nm) per well	$5.6\cdot10^{13}$/$1.9\cdot10^{13}$	$5.6\cdot10^{13}$/$1.9\cdot10^{13}$	$5.6\cdot10^{13}$/$1.9\cdot10^{13}$
Particles per cell	$6.2\cdot10^{9}$	$6.2\cdot10^{9}$	$6.2\cdot10^{9}$
Dye molecules per nanoparticle (*d*=2 nm)	9	5	5
Dye molecules per well	$5.0\cdot10^{14}$/$1.7\cdot10^{14}$	$2.8\cdot10^{14}$/$9.5\cdot10^{13}$	$2.8\cdot10^{14}$/$9.5\cdot10^{13}$
Dye molecules per cell	$5.6\cdot10^{10}$	$3.1\cdot10^{10}$	$3.1\cdot10^{10}$

Nanoparticle uptake studies in 3D cell culture model (spheroids)

Multicellular 3D spheroids of hAs, hPs and hBECs were established for 120 h as described above (3000 cells per well: 1000 hpBECs, 1000 hpPs and 1000 hpAs in 60 µL). After 120 h of spheroid generation, the gold nanoparticles or the corresponding controls (dye alone) were added and incubated for 24 h at 37 °C (Table 1). The spheroids were then washed with DPBS, fixed with 4% paraformaldehyde (Merck), followed by washing for three times with DPBS. Actin was stained with AlexaFluor^{TM}647 according to the manufacturer's recommendation (Thermo Fisher), followed by washing for three times with DPBS. Then the cells were stained with DAPI, washed three times with PBS and imaged by CLSM. To identify the location of the nanoparticles within the spheroids, z-stacks were acquired (step size 5 µm).

Statistics

All cell culture experiments, including spheroids, were performed with at least two independent cell culture experiments with at least three cell samples run in parallel. Data are expressed as the average±standard deviation of the mean for each group. Student's *t*-test was used to compare groups; *p* values less than 0.05 were considered as significant.

Results and Discussion

To track the cellular uptake of the ultrasmall gold nanoparticles, they were first fluorescently labelled. To this end, ultrasmall gold nanoparticles were surface-functionalized by click reaction or by direct functionalization (Figure 1). The reduction of tetrachloroauric acid in the presence of the cysteine-containing azide-modified tripeptide (6-azido-lysine)cysteine-asparagine led to the formation of azide-terminated ultrasmall gold nanoparticles to which the dye was attached in a second step by copper-catalyzed azide-alkyne cycloaddition (CuAAC) [48]. UV-vis spectra of dispersed Au-Click-FAM and Au-CGGpTPAAK-FAM nanoparticles showed the absorption band of fluorescein at 495 nm and for Au-Click-Cy3 nanoparticles the absorption band of Cy3 at 560 nm (see Supplementary Information, Figures S1-S3). Differential centrifugal sedimentation (DCS) gave a hydrodynamic diameter of 1.57±0.62 nm for Au-Click-FAM nanoparticles, 1.53±0.75 nm for Au-Click-Cy3 nanoparticles, and 1.96±0.67 nm for Au-CGGpTPAAK-FAM nanoparticles (Figure 2). The size of the gold core and its shape were assessed by high-resolution transmission electron microscopy (HRTEM). HRTEM analysis of Au-Click-FAM, Au-Click-Cy3 and Au-CGGpTPAAK-FAM nanoparticles showed well-separated mostly spherical nanoparticles with an average size of 2.28±0.38 nm, 1.90±0.18 nm and 1.99±0.59 nm (Figure 3). The strong covalent gold-sulfur bond efficiently prevents a dissociation of the dye ligand from the nanoparticle core, also in biological environment [48, 49]. Note that the hydrodynamic diameter is generally underestimated by DCS for functionalized nanoparticles due to the smaller effective density in dispersion [50].

Due to their small size, ultrasmall gold nanoparticles are well-suited to transport synthetic molecules (like drugs) or biomolecules into the cell and possibly also across the blood-brain barrier. Fluorescent labelling of the nanoparticles allows to localize them inside a cell or a spheroid. First, uptake studies in a 2D co-culture cell model (hBECs, hAs and hPs) were performed with Au-Click-FAM, Au-Click-Cy3 and Au-CGGpTPAAK-FAM nanoparticles, respectively, to study the nanoparticle interaction will the three cell types. In 2D culture, we do

not have a functional blood-brain barrier but only the individual cell types in co-culture. Confocal laser scanning microscopy (z-stack across the cells) showed a strong fluorescence of Au-Click-FAM nanoparticles and Au-Click-Cy3 nanoparticles, also inside the nuclei of all cell types tested as indicated by the colocalization of particle fluorescence and DNA (DAPI) in the focus plane (Figure 4). In contrast, Au-CGGpTPAAK-FAM nanoparticles were taken up by all tested cell types, but they did not enter the nucleus (Figure 5). This indicates that the nanoparticle surface functionalization plays a role for the intracellular processing. Control experiments with the dissolved dyes FAM-alkyne, Cy3-alkyne, and CGGpTPAAK-FAM did not show any cellular uptake, i.e. the dyes alone cannot penetrate the cell membrane (Figure 6). Additional images are shown in the Supplementary Information (Figures S5-S8).

After validating the uptake of the ultrasmall nanoparticles into hBECs, hAs and hPs, their potential to penetrate the three-dimensional spheroid model was assessed. In the first steps, spheroids were generated and their structural properties characterized. Their generation took place in ultra-low attachment plates (ULAP), *i.e.* completely free of any supporting scaffold material for cell organization [7, 17]. The endothelial cells form an outer cell monolayer representing the lumen side, the pericytes line up in between, and the astrocytes accumulate in the core of the spheroids that could be perceived as the parenchymal space. Such spheroids mimic the morphological arrangement of the three cell types in the neurovascular unit (Figure 7) [8, 13, 15, 17].

To show the self-assembly of spheroids with three cell types, hpAs, hpPs, hpBECs were individually labelled with CellTracker and cultivated in the ULAPs for 72-120 h. By variation of the incubation time, we generated spheroids with a diameter between 200 µm and 350 µm (Figure 8). After 120 h of generation the spheroids reached a diameter of about 350 µm with a distinct hierarchical structure where hpBECs were localized at the periphery of the spheroid, hpPs were near the surface, and hpAs formed the core (Figure 9). To evaluate the cell viability in the spheroids, a live/dead assay was performed. The spheroids consisted almost exclusively of viable cells (Figure 9). Nzou *et al.* have shown for a similar spheroid model that the fraction of dead cells remains low until at least 21 days [17].

Immunofluorescent staining for the specific markers, i.e. CD31 (for endothelial cells; hBECs), β-Catenin (for cell-cell contacts), PDGF-rβ (for perictyes, hpPs), GFAP (for astrocytes, hpAs), and ZO-1 (tight junction marker), was performed to study the arrangement of cells and the functionality of the blood-brain barrier (Figure 10; see also Supplementary Information, Figures S9-S12). Fluorescent immunostaining reveals the assembly of the different cell types within the

organoids and shows the localization of marker proteins for the cell types used here. The localization of β-catenin at sites of cell-cell contacts and the expression of the efflux pump P-gp that is specific for endothelial cells was confirmed with the corresponding antibodies. The expression of the tight junction protein ZO-1 was shown by immunostaining (Figure 11).

We studied the integrity and dynamic properties of the barrier formed in the spheroids by incubation with a FITC-conjugated anti-mouse F4/80 antibody or with FITC dye alone. At first, the permeability was evaluated in untreated spheroids. For comparison, we added antibodies or dye after pretreatment with histamine. Histamine is a chemical reagent that can transiently open the BBB [51]. Green fluorescence was detected in organoids after pretreatment with histamine by confocal laser scanning microscopy (Figure 12), but no fluorescence was detected in untreated spheroids, showing that a vascular barrier was indeed present in the spheroids.

The uptake of nanoparticles in 3D cell culture was then tested with 3D BBB spheroids. The main factors that can influence the cellular uptake of nanoparticles and the penetration in spheroids are nanoparticle size, shape, composition and surface functionalization [27, 52-55]. We found that the three kinds of ultrasmall gold nanoparticles (Au-Click-FAM, Au-Click-Cy3 and Au-CGGpTPAAK-FAM) were all able to enter the spheroid, i.e. to cross the vascular barrier. In contrast, the dissolved molecules did not enter the spheroid, in agreement with the 2D experiments (Figure 13 and Supplementary Information, Figures S13 and S14). In the 2D cell culture experiments, it was found that two out of three kinds of nanoparticles also entered the cell nucleus. This is also very likely for the spheroids but cannot be microscopically resolved due to the optical limits of the CLSM for the large spheroids.

The mechanism of the nanoparticle uptake was beyond the scope of this investigation. However, Cho *et al.* examined these BBB spheroids for efflux pump activity, which is responsible for the active transport of a variety of drugs. The transport of brain-penetrating drugs into the spheroids was due to receptor-mediated transcytosis [15]. Whether this is the case in our experiments is not known.

From a toxicological point of view, gold nanoparticles have been extensively investigated [18, 24-26, 41, 47, 56-58]. Depending on size and surface functionalization, the gold nanoparticles can show different effects on cell viability. For instance, Leite *et al.* have demonstrated that some types of gold nanoparticle can promote neurotoxic effects such as neuroinflammation and neurodegeneration in the central nervous system in animal models [18]. However, in most cases gold nanoparticles are considered as safe due to their chemical inertness associated with the noble character of gold [29, 31, 32, 35, 38, 43, 44].

Conclusions

We have presented the synthesis of three kinds of fluorescent ultrasmall surface-functionalized gold nanoparticles. They were applied to two-dimensional and three-dimensional cell cultures (spheroids) of human primary astrocytes, pericytes, and brain endothelial cells. Ultra-low attachment plates were used to generate 3D spheroids with a size of 350 µm. In a 2D co-culture, the three kinds of fluorescent ultrasmall gold nanoparticles were efficiently taken up by the three kinds of primary cells, and they also easily entered the 3D spheroids. The surface functionalization clearly plays a role as it appears to determine whether such nanoparticles can enter the cell nucleus or not. However, it did not influence the passage into spheroids. As a future perspective, ultrasmall gold nanoparticles can serve as carrier system for biomolecules and dyes across the blood-brain barrier. Our results clearly show that dissolved dyes alone did not cross the blood-brain barrier, so that it is easily conceivable that a soluble drug can be transported after attachment to an ultrasmall nanoparticle (instead of a dye as shown here). However, given the small size of the nanoparticles, it is unlikely that they can act as carriers for biomolecules like proteins, DNA, or antibodies which are larger than the carrier itself. An *in vitro* model for such a neurovascular unit is also a valuable platform for the development and testing of new therapeutics in brain neurosciences, *e.g.* for stroke research. From a nanotoxicogical point of view (biodistribution), it is remarkable that such nanoparticles can enter the brain, the brain cells, and even their nucleus.

Acknowledgements

We thank the Deutsche Forschungsgemeinschaft (DFG) for funding within the Collaborative Research Center "Supramolecular Chemistry on Proteins" (SFB 1093).

Data availability

The raw/processed data required to reproduce these findings will be shared upon request.

Figures

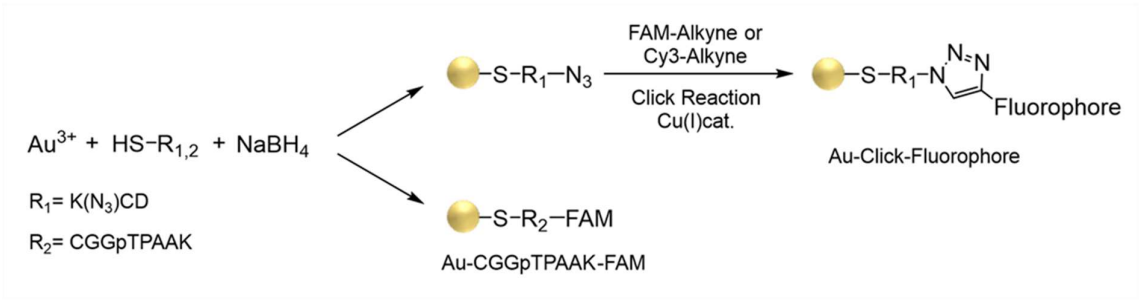

Fig. 1

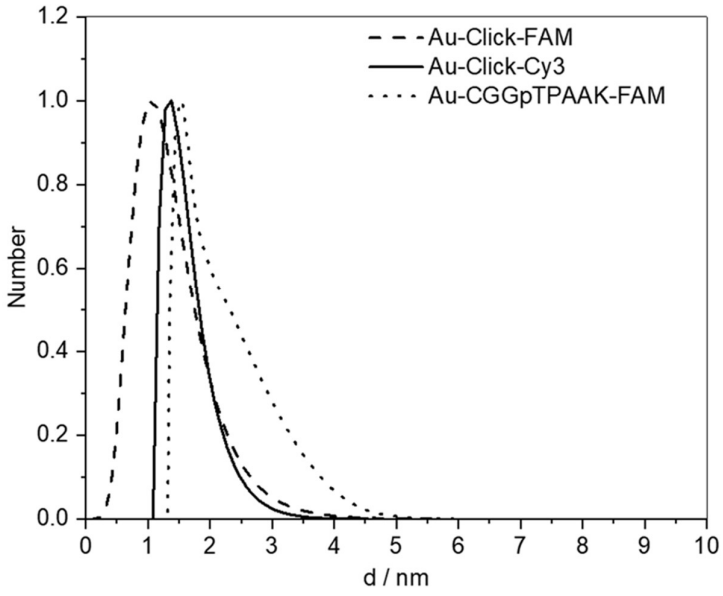

Fig. 2

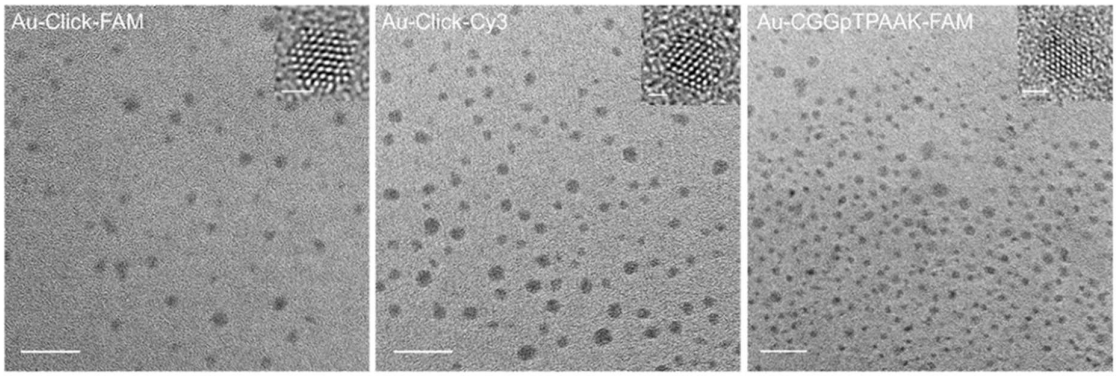

Fig. 3

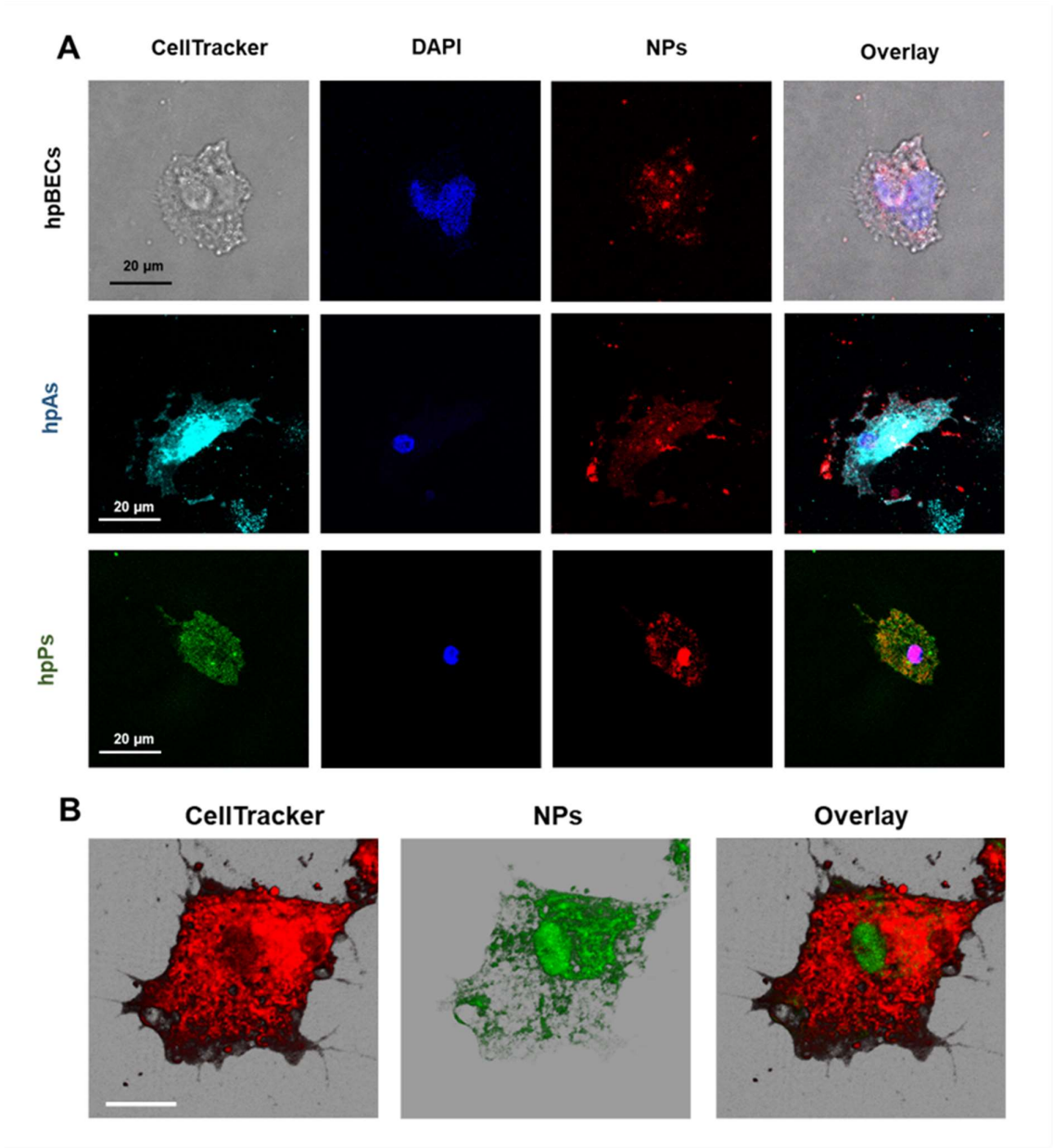
A
CellTracker
DAPI
NPs
Overlay
hpBECs
hpAs
hpPs
20 μm
20 μm
20 μm
B
CellTracker
NPs
Overlay

Fig. 4

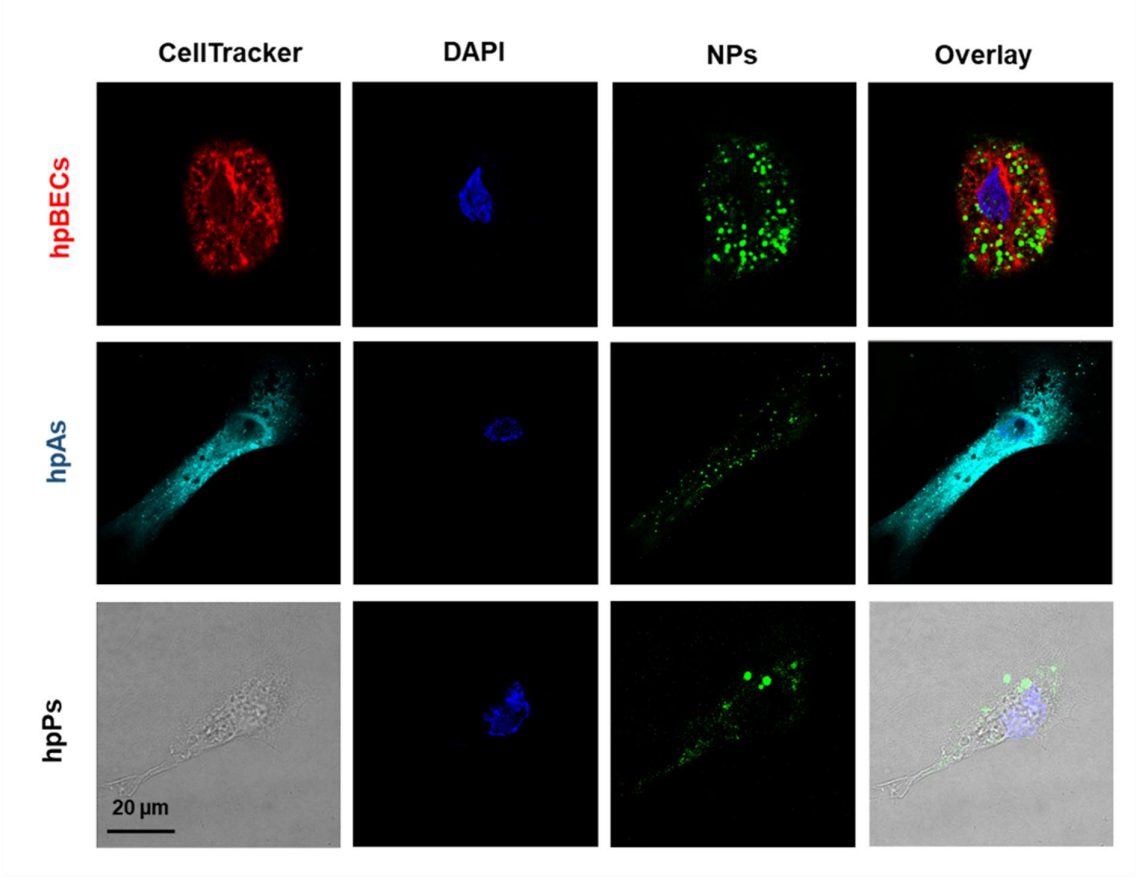

Fig. 5

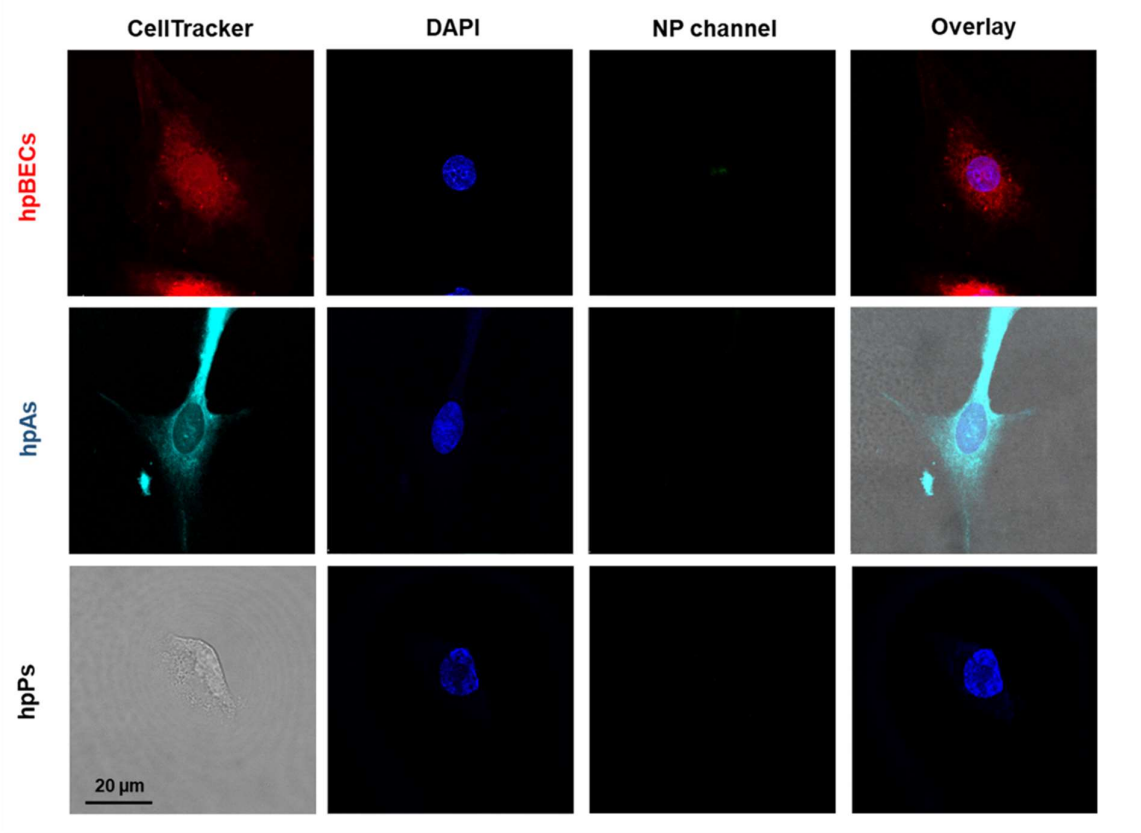
CellTracker
DAPI
NP channel
Overlay
hpBECs
hpAs
hpPs
20 µm

Fig. 6

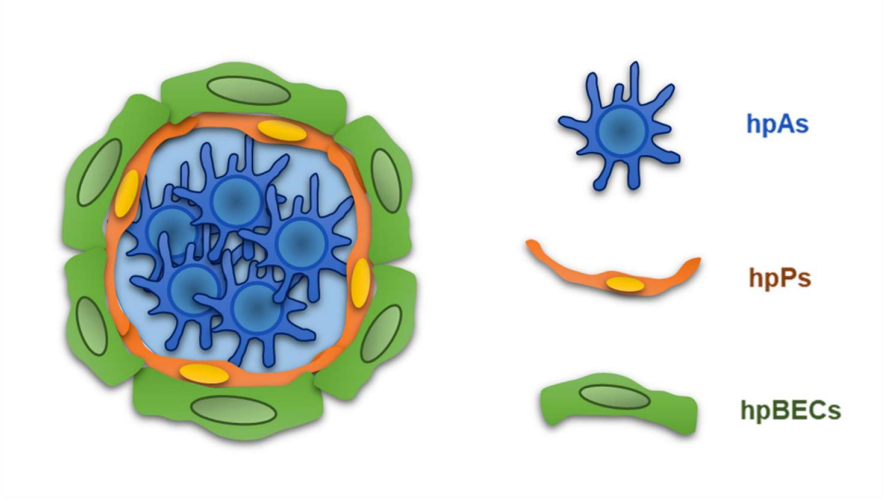
hpAs
hpPs
hpBECs

Fig. 7

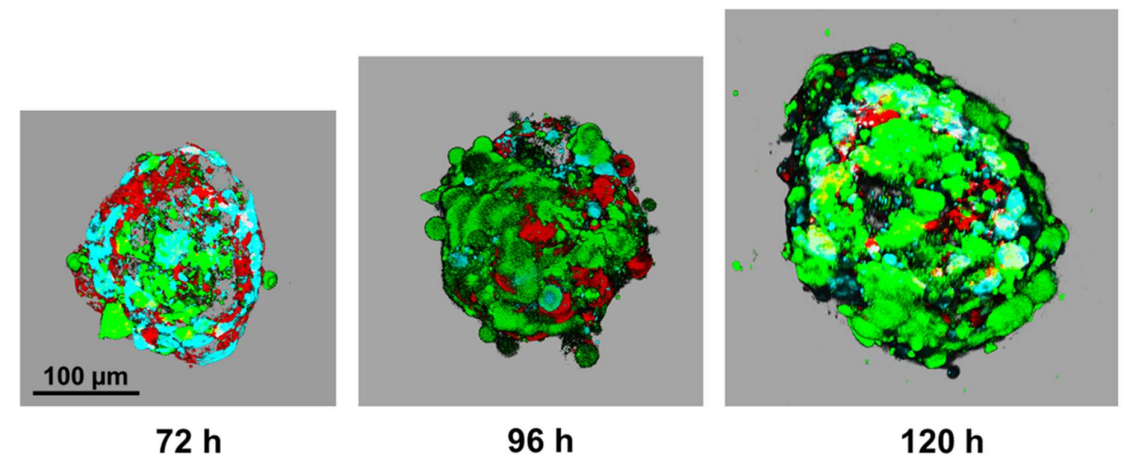

Fig. 8

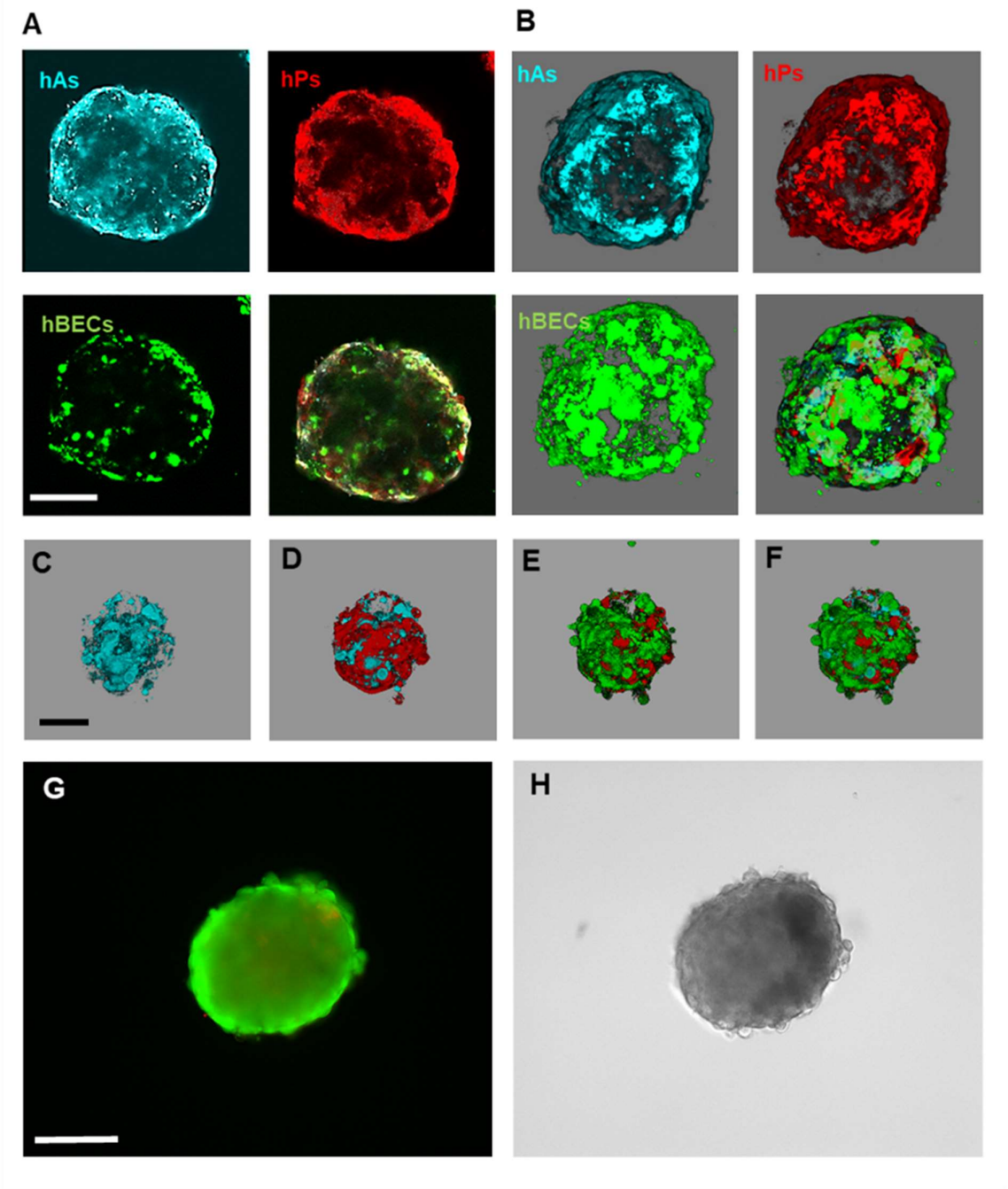

Fig. 9

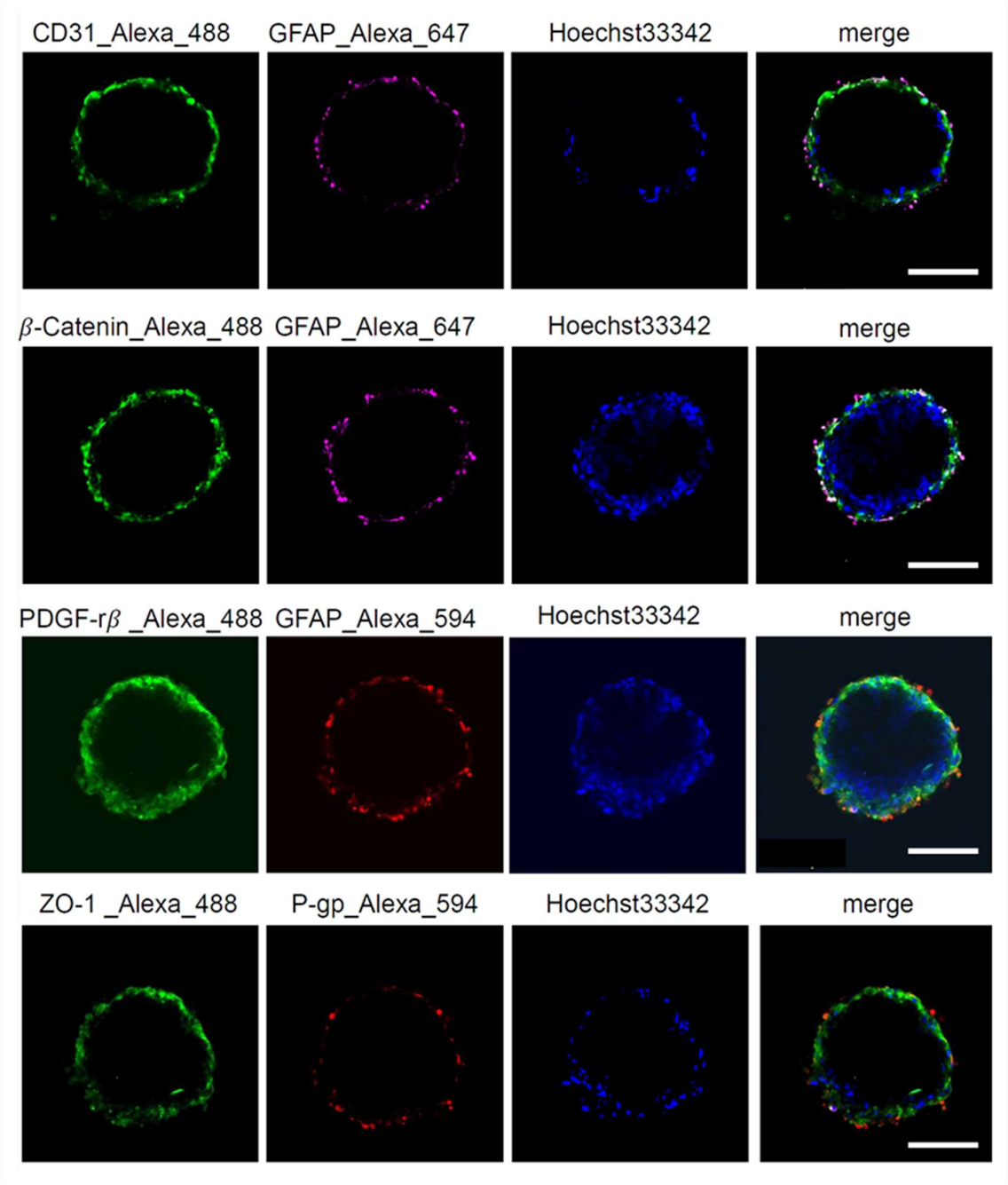
CD31_Alexa_488
GFAP_Alexa_647
Hoechst33342
merge
β-Catenin_Alexa_488
GFAP_Alexa_647
Hoechst33342
merge
PDGF-rβ _Alexa_488
GFAP_Alexa_594
Hoechst33342
merge
ZO-1 _Alexa_488
P-gp_Alexa_594
Hoechst33342
merge

Fig. 10

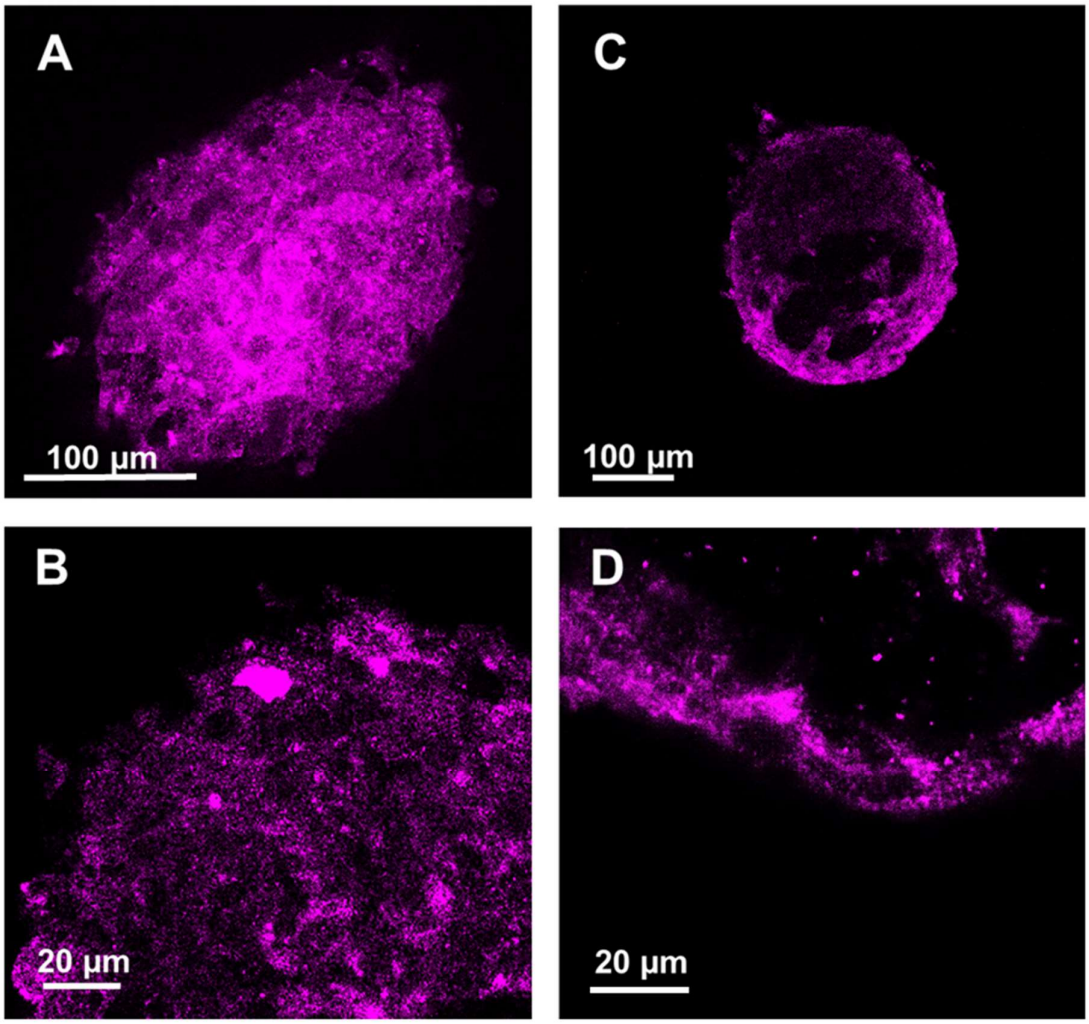

Fig. 11

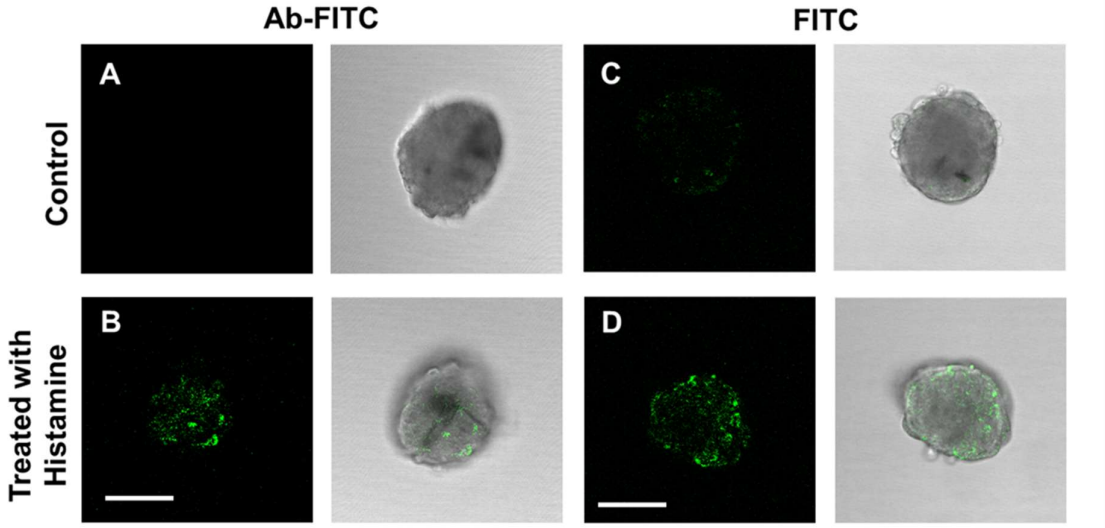

Fig. 12

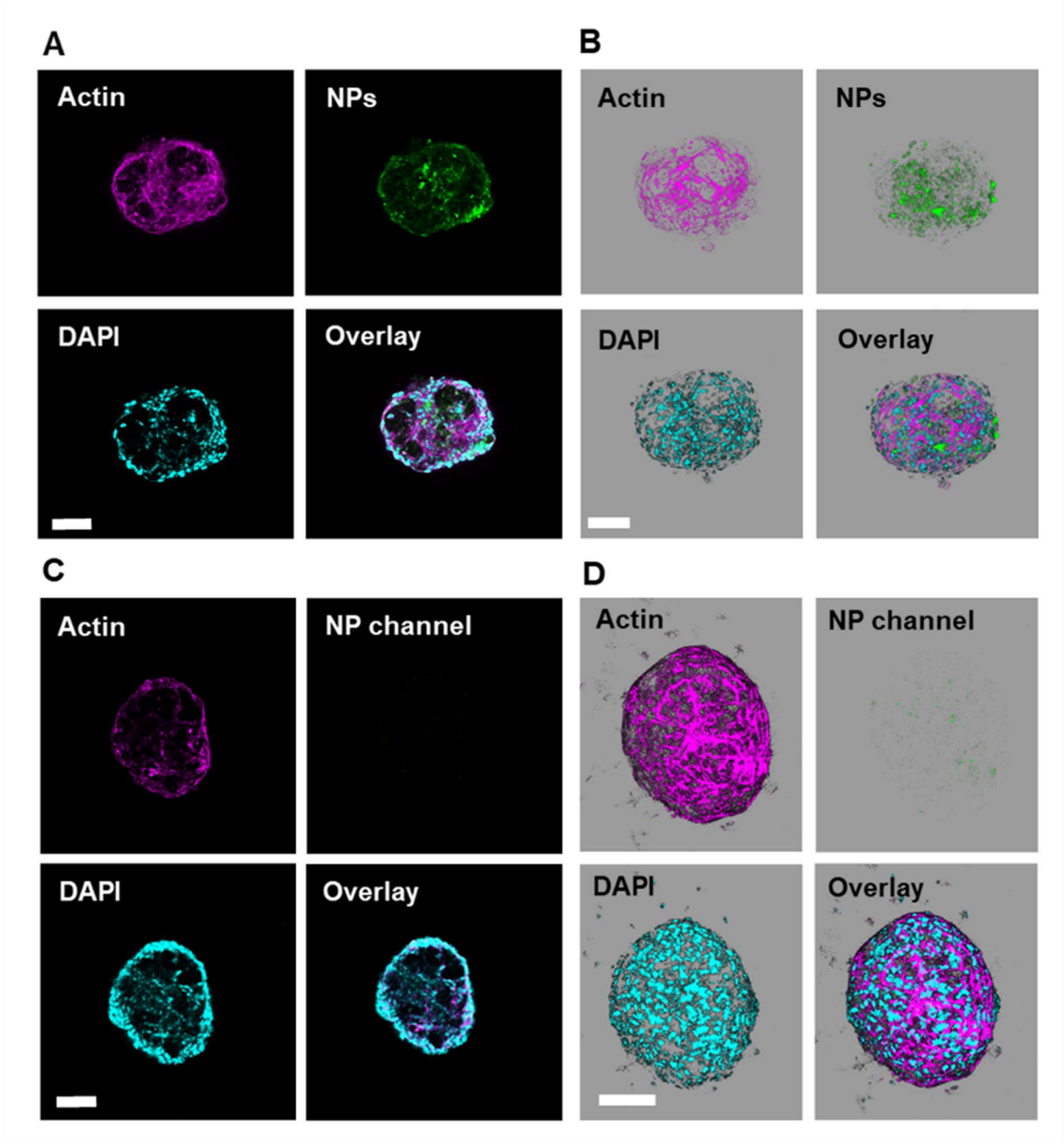
A
Actin
NPs
DAPI
Overlay
B
Actin
NPs
DAPI
Overlay
C
Actin
NP channel
DAPI
Overlay
D
Actin
NP channel
DAPI
Overlay

Fig. 13

Figure captions

Fig. 1. Synthesis pathways of clicked and peptide-functionalized ultrasmall gold nanoparticles. In both cases, the strong covalent bonds between gold, sulfur, and ligand lead to a persistent attachment of the ligand to the gold core.

Fig. 2. Differential centrifugal sedimentation (DCS) data of water-dispersed nanoparticles.

Fig. 3. HRTEM images of Au-Click-FAM, Au-Click-Cy3 and Au-CGGpTPAAK-FAM nanoparticles. Scale bar of the overview image: 10 nm; scale bar of the inset image: 1 nm.

Fig. 4. A: Confocal laser scanning microscopic images to demonstrate the uptake of red-fluorescing Cy3-labelled ultrasmall gold nanoparticles (NPs) by human brain endothelial cells (hBECs, unstained), human astrocytes (hAs, cyan), and human pericytes (hPs, green) after 24 h of incubation in 2D co-culture (metal concentration 25 µg mL^{-1}, *i.e.* 4.5 µg in each well). The particles easily entered all three cell types, including the nucleus. **Blue**: nuclear staining by DAPI; **red**: Au-Click-Cy3 nanoparticles. **B:** The reconstruction of z-stacks (20 slices) in a 3D representation of a human brain endothelial cell after the uptake of Au-Click-FAM nanoparticles demonstrates that the nanoparticles were present inside the cell and the nucleus. Similar images have been recorded for the two other cell types. Scale bar 20 µm.

Fig. 5. Confocal laser scanning microscopic images to demonstrate the uptake of green fluorescing CGGpTPAAK-FAM-conjugated ultrasmall gold nanoparticles (NPs) by human brain endothelial cells (hBECs, red), human astrocytes (hAs, cyan) and human pericytes (hPs, unstained) after 24 h of incubation in co-culture (metal concentration 25 µg $µL^{-1}$, *i.e.* 4.5 µg in each well). The nanoparticles were taken up by the three cell types but did not enter the nucleus. **Blue**: nuclear staining by DAPI; **green**: Au-CGGpTPAAK-FAM nanoparticles.

Fig. 6. Confocal laser scanning microscopic images to analyze the uptake of green fluorescing dissolved CGGpTPAAK-FAM molecules (NP channel) by human brain endothelial cells (hBECs, red), human astrocytes (hAs, cyan) and human pericytes (hPs, unstained) after 24 h of incubation in co-culture ($2.8 \cdot 10^{14}$ dye molecules per well). No fluorescence was detected, i.e.

the molecules did not enter the cells. **Blue**: nuclear staining by DAPI; **green**: CGGpTPAAK-FAM molecules. See SI for the data of the uptake of dissolved FAM-alkyne and Cy3-alkyne.

Fig. 7. Schematic representation of a three-dimensional brain spheroid (diameter about 400 µm) as *in vitro* model for the blood-brain barrier. The spheroid core is composed mainly of human primary astrocytes (hpAs), covered with human primary pericytes (hpPs), while human primary brain endothelial cells (hpBECs) form the surface layer.

Fig. 8. Confocal laser scanning microscopy images of 3D BBB spheroids after 72 h, 96 h, and 120 h of cultivation. The organoids increase in diameter from 200 µm to 350 µm, and the three cell types arrange according to their natural spatial localization in the neurovascular unit. Human astrocytes (hAs, cyan), human pericytes (hPs, red) and human brain endothelial cells (hBECs, green) form the spheroid.

Fig. 9. Representative confocal images showing the organization of human astrocytes (hAs, cyan), human pericytes (hPs, red) and human brain endothelial cells (hBECs, green) after organoid co-culture for 120 h. The images show the organization of the cells at 30 µm depth (z-stack) from the surface of the organoid (**A**). Reconstruction of all z-stacks (20 slices) in a 3D representation of one organoid (**B**). Characterization of organoids: The reconstruction of z-stacks (20 slices) in a 3D representation of a core of organoid consisting of astrocytes (blue, **C**), covered by pericytes (red, **D**) and an outer layer of endothelial cells (green, **E**), and the overlay image of all channels (**F**). Live/dead assay of 3D BBB organoids after 120 h of generation time imaged by fluorescence microscopy (**G**) and bright field microscopy (**H**). Living cells are stained green fluorescent calcein-AM and dead cells are stained by red by EthD-1. Only very few cells in the spheroid are dead. Scale bar 100 µm.

Fig. 10. Representative confocal images of spheroids stained for the specific markers, *i.e.* CD31 (for hBECs), GFAP (for hpAs), β-Catenin (sites of cell-cell contacts), PDGF-rβ (for hpPs), ZO-1 (for tight junctions), and P-gp (endothelial specific efflux pump) after a generation time of 120 h. See SI for additional immunostaining images. Scale bar 100 µm.

Fig. 11. Representative confocal images show the presence of the tight junction marker Zona occludens-1 (ZO-1) on the surface (**A**, **B**) and in 30 µm depth (z-stack) from the surface of the spheroid (**C**, **D**). Generation time 120 h.

Fig. 12. Permeability assessment was done by incubating the 3D BBB spheroids with FITC-labelled antibodies (Ab-FITC; **A**) and dissolved FITC (**C**). The upper row represents spheroids with an uncompromised vascular-type barrier (control), and the lower row shows spheroids that were treated with histamine to transiently open the vascular-type barrier. The blood-brain barrier is impermeable for the antibody (**B**) and for the dissolved dye (**D**) but becomes permeable in the presence of histamine. Scale bars 100 µm.

Fig. 13. Representative confocal images of 3D organoids (120 h cultivation time), showing actin (magenta), Au-Click-FAM nanoparticles (green), and DAPI (cyan). The distribution of the nanoparticles at 30 µm depth (z-stack) from the surface of the spheroid is shown in **A** and **C**. The reconstruction of all z-stacks (20 slices) in a 3D representation is shown in **B** and **D**. Au-Click-FAM nanoparticles readily enter the spheroid, i.e. they penetrated the vascular barrier (**A** and **B**). For FAM-alkyne alone, no green fluorescence was detected, indicating that the dissolved dye alone cannot enter the organoid (**C** and **D**). Scale bar 100 µm. See SI for the corresponding experiments with Au-Click-Cy3 and Au-CGGpTPAAK-FAM nanoparticles.

References

[1] Cecchelli R, Berezowski V, Lundquist S, Culot M, Renftel M, Dehouck MP FL. Modelling of the blood-brain barrier in drug discovery and development. Nat Rev Drug Discov 2007;6:650-61.

[2] Saraiva C, Praça C, Ferreira R, Santos T, Ferreira L, Bernardino L. Nanoparticle-mediated brain drug delivery: Overcoming blood-brain barrier to treat neurodegenerative diseases. J Control Rel 2016;235:34-47.

[3] Helms HC, Abbott NJ, Burek M, Cecchelli R, Couraud PO, Deli MA, Förster C, Galla HJ, Romero IA, Shusta EV, Stebbins MJ, Vandenhaute E, Weksler B, Brodin B. In vitro models of the blood-brain barrier: An overview of commonly used brain endothelial cell culture models and guidelines for their use. J Cereb Blood Flow Metab 2016;36:862-90.

[4] Iadecola C. The neurovascular unit coming of age: A journey through neurovascular coupling in health and disease. Neuron 2017;96:17-42.

[5] Lu H, Stenzel MH. Multicellular tumor spheroids (MCTS) as a 3D in vitro evaluation tool of nanoparticles. Small 2018;14:e1702858.

[6] Pandey PK, Sharma AK, Gupta U. Blood brain barrier: An overview on strategies in drug delivery, realistic in vitro modeling and in vivo live tracking. Tissue Barr 2015;4:e1129476.

[7] Nzou G, Seeds MC, Wicks RT, Atala AJ. Fundamental neurovascular components for the development of complex and dynamic in vitro brain equivalent models. J Alzheimers Neurodegener Dis 2019;5:021.

[8] Bergmann S, Lawler SE, Qu Y, Fadzen CM, Wolfe JM, Regan MS, Pentelute BL, Agar NYR, Cho CF. Blood–brain-barrier organoids for investigating the permeability of CNS therapeutics. Nat Protoc 2018;13:2827-43.

[9] Upadhyay RK. Drug delivery systems, CNS protection, and the blood brain barrier. Biomed Res Int 2014;2014:869269.

[10] Agundez JA, Jiménez-Jiménez FJ, Alonso-Navarro H, García-Martín E. Drug and xenobiotic biotransformation in the blood-brain barrier: a neglected issue. Front Cell Neurosci 2014;8:335.

[11] Hatherell K, Couraud PO, Romero IA, Weksler B, Pilkington GJ. Development of a three-dimensional, all-human in vitro model of the blood-brain barrier using mono-, co-, and tri-cultivation Transwell models. J Neurosci Methods 2011;199:223-9.

[12] Lancaster MA, Renner M, Martin CA, Wenzel D, Bicknell LS, Hurles ME, Homfray T, Penninger JM, Jackson AP, Knoblich JA. Cerebral organoids model human brain development and microcephaly. Nature 2013;501:373-9.

[13] Urich E, Patsch C, Aigner S, Graf M, Iacone R, Freskgård PO. Multicellular self-assembled spheroidal model of the blood brain barrier. Sci Rep 2013;3:1500.

[14] Hanada S, Fujioka K, Inoue Y, Kanaya F, Manome Y, Yamamoto K. Cell-based in vitro blood-brain barrier model can rapidly evaluate nanoparticles' brain permeability in association with particle size and surface modification. Int J Mol Sci 2014;15:1812-25.

[15] Cho CF, Wolfe JM, Fadzen CM, Calligaris D, Hornburg K, Chiocca EA, Agar NYR, Pentelute BL, Lawler SE. Blood-brain-barrier spheroids as an in vitro screening platform for brain-penetrating agents. Nat Commun 2017;8:15623.

[16] Cho H, Seo JH, Wong KHK, Terasaki Y, Park J, Bong K, Arai K, Lo EH, Irimia D. Three-dimensional blood-brain barrier model for in vitro studies of neurovascular pathology. Sci Rep 2015;5:15222.

[17] Nzou G, Wicks RT, Wicks EE, Seale SA, Sane CH, Chen A, Murphy SV, Jackson JD, Atala AJ. Human cortex spheroid with a functional blood brain barrier for high-throughput neurotoxicity screening and disease modeling. Sci Rep 2018;8:7413.

[18] Leite PEC, Pereira MR, Harris G, Pamies D, Dos Santos LMG, Granjeiro JM, Hogberg HT, Hartung T, Smirnova L. Suitability of 3D human brain spheroid models to distinguish toxic effects of gold and poly-lactic acid nanoparticles to assess biocompatibility for brain drug delivery. Part Fibre Toxicol 2019;16.
[19] Georgieva JV, Kalicharan D, Couraud PO, Romero IA, Weksler B, Hoekstra D, Zuhorn IS. Surface characteristics of nanoparticles determine their intracellular fate in and processing by human blood-brain barrier endothelial cells in vitro. Mol Ther 2011;19:318-25.
[20] Prades R, Guerrero S, Araya E, Molina C, Salas E, Zurita E, Selva J, Egea G, López-Iglesias C, Teixidó M, Kogan MJ, Giralt E. Delivery of gold nanoparticles to the brain by conjugation with a peptide that recognizes the transferrin receptor. Biomaterials 2012;33:7194-205.
[21] Kong SD, Lee J, Ramachandran S, Eliceiri BP, Shubayev V, I., Lal R, Jin S. Magnetic targeting of nanoparticles across the intact blood-brain barrier. J Control Release 2012;164:49-57.
[22] Jiang W, Xie H, Ghoorah D, Shang Y, Shi H, Liu F, Yang X, Xu H. Conjugation of functionalized SPIONs with transferrin for targeting and imaging brain glial tumors in rat model. PLoS One 2012;7:e37376.
[23] Shilo M, Motiei M, Hana P, Popovtzer R. Transport of nanoparticles through the blood-brain barrier for imaging and therapeutic applications. Nanoscale 2014;6:2146-52.
[24] Bulcke F, Thiel K, Dringen R. Uptake and toxicity of copper oxide nanoparticles in cultured primary brain astrocytes. Nanotoxicology 2014;8:775-85.
[25] Yang Z, Liu Z, Allaker RP, Reip P, Oxford J, Ahmad Z, Ren G. A review of nanoparticle functionality and toxicity on the central nervous system. J R Soc Interface 2010;7:411-22.
[26] Schmid G, Kreyling WG, Simon U. Toxic effects and biodistribution of ultrasmall gold nanoparticles. Arch Toxicol 2017;91:3011-37.
[27] Nazarenus M, Zhang Q, Soliman MG, del Pino P, Pelaz B, Carregal-Romero S, Rejman J, Rothen-Rutishauser B, Clift MJD, Zellner R, Nienhaus GU, Delehanty JB, Medintz IL, Parak WJ. In vitro interaction of colloidal nanoparticles with mammalian cells: What have we learned thus far? Beilstein J Nanotechnol 2014;5:1477-90.
[28] Mahon E, Salvati A, Bombelli FB, Lynch I, Dawson KA. Designing the nanoparticle–biomolecule interface for "targeting and therapeutic delivery". J Control Release 2012;161:164-74.
[29] Yeh YC, Creran B, Rotello VM. Gold nanoparticles: preparation, properties, and applications in bionanotechnology. Nanoscale 2012;4:1871-80.
[30] Lu Y, Chen W. Sub-nanometre sized metal clusters: from synthetic challenges to the unique property discoveries. Chem Soc Rev 2012;41:3594-623.
[31] Dykman L, Khlebtsov N. Gold nanoparticles in biomedical applications: recent advances and perspectives. Chem Soc Rev 2012;41:2256-82.
[32] Dreaden EC, Alkilany AM, Huang X, Murphy CJ, El-Sayed MA. The golden age: gold nanoparticles for biomedicine. Chem Soc Rev 2012;41:2740-79.
[33] Leifert A, Pan-Bartnek Y, Simon U, Jahnen-Dechent W. Molecularly stabilised ultrasmall gold nanoparticles: synthesis, characterization and bioactivity. Nanoscale 2013;5:6224-42.
[34] Mathaes R, Winter G, Besheer A, Engert J. Non-spherical micro- and nanoparticles: fabrication, characterization and drug delivery applications. Exp Opin Drug Deliv 2015;12:481-92.
[35] Chinen AB, Guan CM, Ferrer JR, Barnaby SN, Merkel TJ, Mirkin CA. Nanoparticle probes for the detection of cancer biomarkers, cells, and tissues by fluorescence. Chem Rev 2015;115:10530-74.

[36] Rotello VM. Organic chemistry meets polymers, nanoscience, therapeutics and diagnostics. Beilstein J Org Chem 2016;12:1638-46.
[37] Zarschler K, Rocks L, Licciardello N, Boselli L, Polo E, Garcia KP, De Cola L, Stephan H, Dawson KA. Ultrasmall inorganic nanoparticles: State-of-the-art and perspectives for biomedical applications. Nanomedicine 2016;12:1663-701.
[38] Gupta A, Moyano DF, Parnsubsakul A, Papadopoulos A, Wang LS, Landis RF, Das R, Rotello VM. Ultrastable and biofunctionalizable gold nanoparticles. ACS Appl Mater Interfaces 2016;8:14096-101.
[39] Kopp M, Kollenda S, Epple M. Nanoparticle–protein interactions: Therapeutic approaches and supramolecular chemistry. Acc Chem Res 2017;50:1383-90.
[40] Mout R, Ray M, Tay T, Sasaki K, Tonga GY, Rotello VM. General strategy for direct cytosolic protein delivery via protein-nanoparticle co-engineering. ACS Nano 2017;11:6416-21.
[41] Huo S, Jin S, Ma X, Xue X, Yang K, Kumar A, Wang PC, Zhang J, Hu Z, Liang XJ. Ultrasmall gold nanoparticles as carriers for nucleus-based gene therapy due to size-dependent nuclear entry. ACS Nano 2014;8:5852-62.
[42] Vincenzo A, Roberto P, Marco F, Onofrio MM, Maria Antonia I. Surface plasmon resonance in gold nanoparticles: a review. J Phys C: Condensed Matter 2017;29:203002.
[43] Dykman LA, Khlebtsov NG. Multifunctional gold-based nanocomposites for theranostics. Biomaterials 2016;108:13-34.
[44] Saha K, Agasti SS, Kim C, Li X, Rotello VM. Gold nanoparticles in chemical and biological sensing. Chem Rev 2012;112:2739-79.
[45] Drommelschmidt K, Serdar M, Bendix I, Herz J, Bertling F, Prager S, Keller M, Ludwig AK, Duhan V, Radtke S, de Miroschedji K, Horn PA, van de Looij Y, Giebel B, Felderhoff-Muser U. Mesenchymal stem cell-derived extracellular vesicles ameliorate inflammation-induced preterm brain injury. Brain Behav Immun 2017;60:220-32.
[46] Ruff J, Hüwel S, Kogan MJ, Simon U, Galla HJ. The effects of gold nanoparticles functionalized with ß-amyloid specific peptides on an in vitro model of blood-brain barrier. Nanomedicine: NBM 2017;13:1645-52.
[47] Leite PE, Pereira MR, Granjeiro JM. Hazard effects of nanoparticles in central nervous system: Searching for biocompatible nanomaterials for drug delivery. Toxicol In Vitro 2015;29:1653-60.
[48] van der Meer SB, Loza K, Wey K, Heggen M, Beuck C, Bayer P, Epple M. Click chemistry on the surface of ultrasmall gold nanoparticles (2 nm) for covalent ligand attachment followed by NMR spectroscopy. Langmuir 2019;35:7191-204.
[49] Ruks T, Beuck C, Schaller T, Niemeyer F, Zähres M, Loza K, Heggen M, Hagemann U, Mayer C, Bayer P, Epple M. Solution NMR spectroscopy with isotope-labelled cysteine (^{13}C, ^{15}N) reveals the surface structure of L-cysteine-coated ultrasmall gold nanoparticles (1.8 nm). Langmuir 2019;35:767-78.
[50] Fissan H, Ristig S, Kaminski H, Asbach C, Epple M. Comparison of different characterization methods for nanoparticle dispersions before and after aerosolization. Anal Meth 2014;6:7324-34.
[51] Abbott NJ. Inflammatory mediators and modulation of blood-brain barrier permeability. Cell Mol Neurobiol 2000;20:131-47.
[52] Chitrani BD, Ghazani AA, Chan WCW. Determining the size and shape dependence of gold nanoparticle uptake into mammalian cells. Nano Lett 2006;6:662-8.
[53] He C, Hu Y, Yin L, Tang C, Yin C. Effects of particle size and surface charge on cellular uptake and biodistribution of polymeric nanoparticles. Biomaterials 2010;31:3657-66.
[54] Canton I, Battaglia G. Endocytosis at the nanoscale. Chem Soc Rev 2012;41:2718-39.

[55] Sahay G, Alakhova DY, Kabanov AV. Endocytosis of nanomedicines. J Contr Rel 2010;145:182-95.
[56] Chueh PJ, Liang RY, Lee YH, Zeng ZM, Chuang SM. Differential cytotoxic effects of gold nanoparticles in different mammalian cell lines. J Hazard Mater 2014;264:303-12.
[57] Leite PEC, Pereira MR, Santos CAN, Campos PC, Esteves TM, Granjeiro JM. Gold nanoparticles do not induce myotube cytotoxicity but increase the susceptibility to cell death. Toxicol in Vitro 2015;29:819-27.
[58] Chuang SM, Lee YH, Liang RY, Roam GD, Zeng ZM, Tu HF, Wang SK, Chueh PJ. Extensive evaluations of the cytotoxic effects of gold nanoparticles. Biochim Biophys Acta 2013 1830:4960-73.